International Journal of Geo-Energy

Int. J. Geo-Energy 2023.1(4)
ISSN：2958-2857
https://doi.org/10.58531/ijge103100004

Article

Shear Nonlinear Behavior of Rock Discontinuities with Different Joint Roughness Coefficients

Pengtao He [1], Chaoran Li [2], Wei Zheng [3,*]

[1] School of Mechanical Engineering, Nanjing University of Science and Technology, Nanjing 210094, China;
[2] Department of Civil, Environmental and Geomatic Engineering, University College London, London WC1E 6BT, UK;
[3] School of Civil Engineering, Tongji University, Shanghai 200092, China; 2311847@tongji.edu.cn

Academic Editor: Prof. Dr. Chun Zhu < zhu.chun@hhu.edu.cn>

Received: 20, October, 2023; Revised: 3, November, 2023; Accepted: 3, November, 2023; Published: 7, November, 2023

Abstract: To study the shear failure behavior of rock discontinuity, direct shear tests are carried out on artificial rock discontinuity samples with different roughness under various normal stresses, the influence of roughness on the strength of rock discontinuity is studied, the nonlinear characteristics of rock discontinuity shear are studied according to the variation of shear stiffness. The results indicated that the strength of the rock discontinuity increases with the increase of roughness and exhibited a good linear relationship. With the increase of roughness, the peak value of shear deformation curve becomes more obvious, and the shear failure mode gradually changes from "abrasion" to "cutting ". With an increase in the normal stress and JRC, the energy stored in the sample increased, and the crack development rate from stable to unstable increased.

Keywords: Rock discontinuity; Shear failure behavior; Nonlinear feature; Roughness; Shear stiffness

1. Introduction

The major difference between a rock mass and a general medium is that the former is a multi-fracture body with a certain structure cut by discontinuities. Practices in hydropower, highway, and municipal engineering indicate that the strength of intact rock is not the main cause of rock mass damage. Therefore, studying the mechanical properties of discontinuities

Citation: He P., Li C., Zheng W. Shear Nonlinear Behavior of Rock Discontinuities with Different Joint Roughness Coefficients. *Int. J. Geo-Energy*, 2023, 1(4), doi: 10.58531/ijge103100004

is of great significance for evaluating the safety of rock-related engineering and stability during the operation period.

Instantaneous shear behavior is the most basic mechanical property of discontinuities, and the representative strength characteristics of discontinuities are the three strength formulas, such as the Patton formula [1], Ladanyi formula [2] and Barton formula [3,4]. The vast majority of subsequent research is based on these three strength formulas [3,4]. Compared to the study of the strength characteristics of discontinuities, research on the deformation characteristics of discontinuities is not comprehensive or in-depth. Currently, two main stress paths are used in the shear test of rock discontinuities: one is the conventional discontinuity shear test with constant normal stress and grading increasing shear stress to study the shear deformation characteristics of discontinuities, and the other is a test carried out through normal loading or normal cyclic loading and unloading to study the normal closure characteristics of discontinuities. Many researchers have conducted closure tests on different rock discontinuities, and the shapes of the obtained closure test curves are the same (i.e., these closure curves have highly nonlinear characteristics). Goodman [5,6] attributed most of the nonlinearity of the closure curve to nonlinear crushing and cracking of contiguous asperities, and they considered the unloading curve of the discontinuity to be the same as that of an intact rock. Ji et al. [7] presented a mathematical description of the surface morphology and closure deformation behavior of discontinuities. In addition, to describe the normal closure deformation properties of discontinuities, Goodman used hyperbolic functions, Bandis et al. [8]and Barton et al. [9] used an improved hyperbolic function, Sharp [10] used a semi-logarithmic function, Sun [11] used a power function, and Malama [12] used an exponential function. Zhao et al. [13] considered that natural discontinuities deformed many times in a long geological history; thus, it was reasonable to adopt the hyperbolic elastic model (i.e., the constitutive relation of the normal unloading curve was the same as that of the loading curve). Jing et al. [14] assumed that the stress-displacement relationship was linear in the unloading stage, in which it was linearly unloaded in the tangential direction of the loading curve, and the hyperbolic function was still used in the reloading stage. Yin et al. [15] considering the effects of abrasion on the friction and dilatancy characteristics of the rock discontinuity, established a new shear constitutive model of the rock discontinuity, and reflected the characteristics of tangential cyclic loading. Du et al. [16]discussed the shear deformation characteristics of discontinuities and their dependence on the deformation history using shear tests on artificial rock discontinuities. The test results indicated that the discontinuous surface became increasingly smoother after undergoing different shear deformation histories, and the disparate shear displacement mainly affected the shear strength and had little effect on the dilatancy. Huang et al [17]. studied the effects of undulation Angle and normal stress on shear failure behavior of rock joint by using numerical simulation method.

The factors affecting the mechanical properties of discontinuities vary, and the mechanical properties of discontinuities are not only related to the combined state of rock and discontinuities but are also affected by the surface morphology of the discontinuity surface [7], which is mainly reflected in the influence of surface roughness on its strength and

deformation. Barton and Choubey [3] provided 10 typical profiles and proposed that the roughness of discontinuities varied between 0 and 20 based on a mass of shear test data of natural discontinuities. They introduced the concept of the joint roughness coefficient (JRC) on the basis of studies on the mechanical behavior of discontinuities with different surface morphologies [18]. Because the standard section line was derived from a natural joint and was simple and easy to operate compared with other roughness evaluation methods, the above section lines have been widely used for the assessment of joint roughness [19]. In this study, with four representative Barton standard section lines (Nos. 1, 2, 6, and 6), different JRC specimens were fabricated from cement mortar, and shear tests under various normal stresses were conducted. The influence of the surface morphology of the discontinuities on the shear deformation characteristics was studied, and the nonlinear characteristics and formation mechanism of the shear deformation were discussed, laying the foundation for further research.

2. Methodology

2.1. Sample

Natural rock discontinuities are heterogeneous and anisotropic, and it is difficult to identify discontinuities with identical surface morphologies. In addition, conducting reproducible direct shear tests of discontinuities is difficult because of sampling constraints. The use of a simulated material can not only overcome the above shortcomings, but also properly simulate the geological environment, loading mode, and failure characteristics of discontinuities, making it a significant means for studying its mechanical properties [20]. To study the shear strength and shear deformation of discontinuities, Patton [1] and Einstein et al. [21] used gypsum-simulated materials, Li et al [22], Shen et al. [23], and Wang et al. [24] used a cement mortar simulated material, and Bandis et al. [25] used a model material mixed with barite, bauxite, sand, and water. Du et al. [20] investigated the aforementioned materials and developed a simulated material mixed with high-strength cement, silicon powder, superplasticizer, standard sand, and water.

In this study, we investigated the influence of the surface morphology of a hard structural surface on its shear deformation characteristics to obtain more regular results by using simulated materials. Cement mortar is the most widely used artificial rock-like material because its structure is similar to that of rock. Further, it exhibits stable properties, strong repeatability, and a relatively simple production ratio. This test cement mortar consisted of 325 cement, standard sand, and water with a mix ratio of 2:4:1. The sample was evenly stirred according to the mixture ratio. After it had been fully vibrated on the shaking table, the upper surface of the sample was smooched, the sample was left for 24 h, the mold was removed, and the sample was placed in a standard curing room for curing. The curing temperature was 20 ± 1 °C, the curing humidity was greater than 95%, and the related test was carried out 28 days after curing, as shown in Figure 1. The dimensions of the test blocks were 10 cm × 10 cm × 10 cm. Figure 2 shows the steel molds required for processing the sample and completed cement mortar test block.

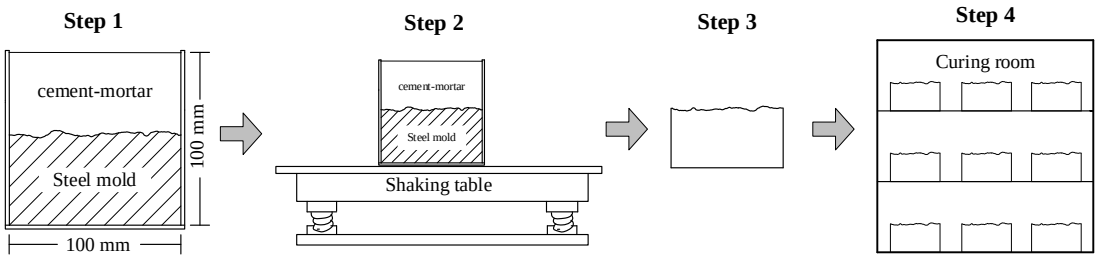

Figure 1. Sample preparation process

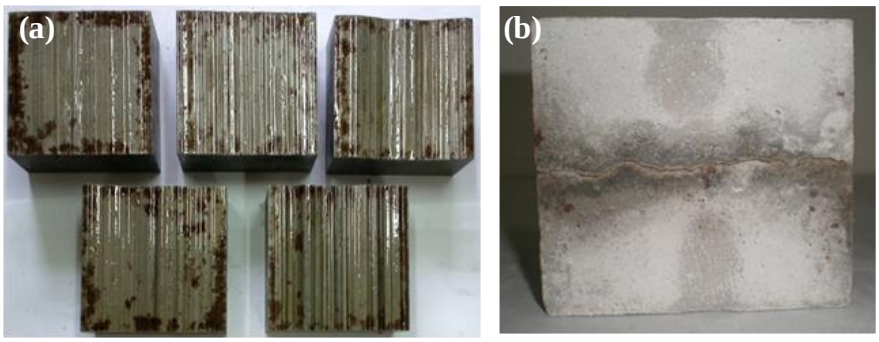

Figure 2. Part of steel mold and cement mortar specimen: (a) steel mold; (b) sample

The surface morphology of a natural rock mass rock discontinuity considerably varies in nature, and its diversity and differences are not conducive to the summary and induction of the law. Therefore, cement mortar was selected as the test material in this study. Sections 1, 4, 6, and 10 of the 10 standard section lines proposed by Patton (Figure 3) were processed into steel molds, and the specimens were poured. Analyzing the test results is difficult because the roughness of the standard profile line proposed by Patton is a range value. Therefore, the roughness of the structural plane adopted in this study was selected as an intermediate value of the range. For example, the roughness of No. 1 rock discontinuity was 0–2, and the roughness was 1 in this study. In addition, for comparison, the flat surface of the structure (JRC = 0) and a complete cube cement mortar test block were poured using the same method.

To elucidate the physical and mechanical properties of the cement mortar specimens, the basic physical and mechanical properties of completely poured specimens were tested. The test results are listed in Table 1. The failure mode in the uniaxial compressive strength test was brittleness.

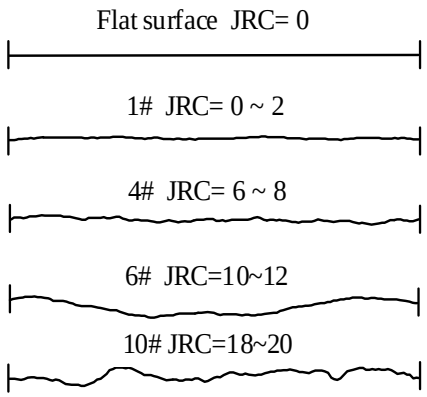

Figure 3. Barton's profile line used in the test

Table 1. Basic mechanical parameters of cement mortar specimens

Density (g/cm^2)	Void ratio	Uniaxial compressive strength (MPa)	Cohesion (MPa)	Frictional angle (°)	Elasticity modulus (GPa)	Poisson's ratio
2.05	0.2	21.73	4.05	49.23	7.9	0.23

2.2. Test Equipment

A CSS-1950 rock biaxial rheological testing machine developed by the Changchun Testing Machine Research Institute was used, as shown in Figure 4. The testing machine adopted bidirectional pressure servo control. The maximum vertical and horizontal stresses provided by the device are 300 kN and 500 kN respectively. The deformation values of both sides of the sample were simultaneously measured, and the deformation was measured using two sets of linear variable differential transformer (LVDT) displacement sensors. The deformation measurement accuracy was 0.001 mm, which can realize the two methods of stress rate control and deformation rate control.

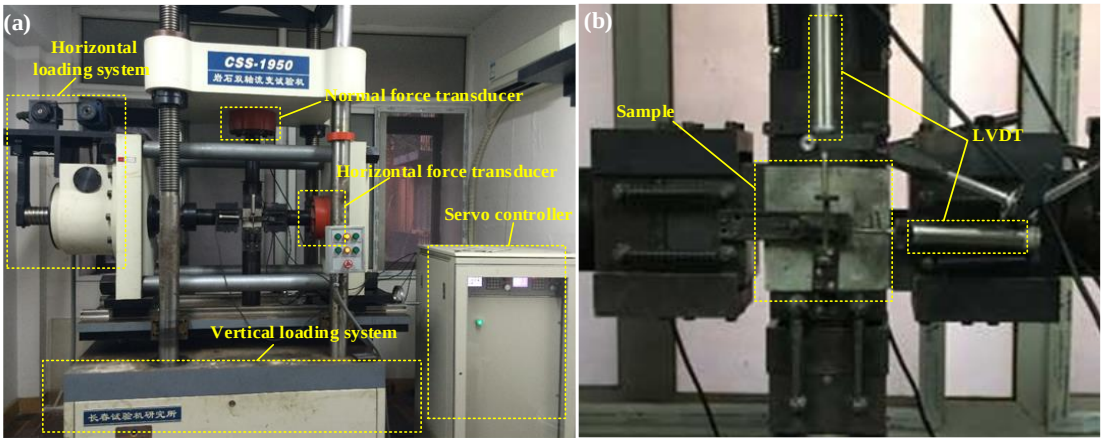

Figure 4. (a) CSS-1950 rock biaxial rheological testing machine;(b) Sample and monitoring system

2.3 Test Progress

This test is a normal stress direct shear test; under a certain normal stress, a shear load parallel to the rock discontinuity is applied to obtain the stress–deformation curve. Twenty groups of rock discontinuity shear test results are obtained with four different normal stresses and five different JRC values. The shear test of the rock mass rock discontinuity adopts roughness of 0, 1, 7, 11, and 19 (flat plate and Barton standard section line No. 1, 4, 6, and 10) and the complete cube test block as test samples. Normal loads of 10%, 15%, 20%, 30%, and 40% of the uniaxial compressive strengths of the materials were applied. The shear rates of the sample was 0.5 MPa /min until it was destroyed. During the tests, high-speed photography was used to record the crack propagation process on the outer surface of the rock discontinuity.

3. Results and Discussion

3.1 Shear Strength Variation Characteristics of Discontinuities with Different Joint Roughness Coefficients

Table 2 shows the results of direct shear tests of rock discontinuity samples under different stresses. As shown in Figure 5, with an increase in the normal stress, the ratio of the shear strength of each rock discontinuity to that of the intact rock block also increased (i.e., with an increase in the normal stress, the difference between the shear strength of the rock discontinuity and that of the intact rock block decreased). This is because of the increase in normal stress, and the percentage born by the shear resistance component generated between the shear teeth in the rock discontinuity resistance increases (i.e., the shear area ratio [24] increases), and the shear strength of the rock discontinuity is closer to that of the intact test block. As shown in Figure 6, with an increase in the JRC, the shear strength of the test block also gradually increases, showing a linearly increasing trend.

Table 2 Shear strength of different specimens

σ (MPa)	τ (MPa)					
	JRC=0	JRC=1	JRC=7	JRC=11	JRC=19	Complete specimen
2.17	1.36	1.76	2.2	2.71	3.58	6.21
3.26	2.55	2.83	2.7	3.31	4.22	7.21
4.35	3.84	3.89	4.54	5.15	6.25	8.37
6.52	4.41	4.73	5.31	7.19	7.9	10.21
8.69	5.8	6.42	7.16	8.11	10.54	12.28

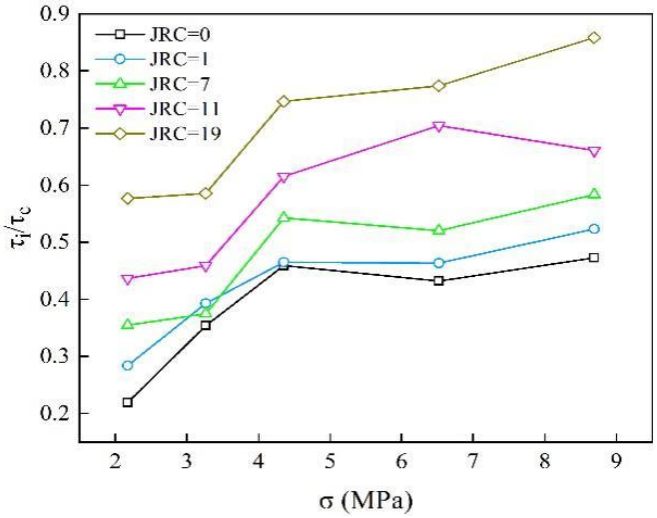

Figure 5. Relationship between shear strength ratio and normal stress

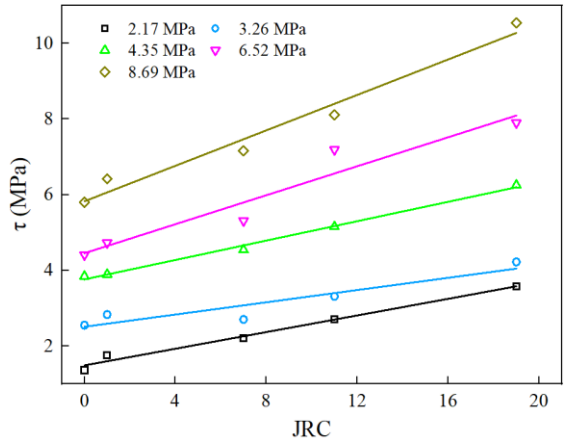

Figure 6. Relationship between JRC and shear strength

According to Coulomb's law, the shear strength parameters under different JRC conditions, namely cohesion (c) and friction angle (φ) could be obtained. As shown in Figure 7, the cohesive force and friction angle linearly increased with the JRC.

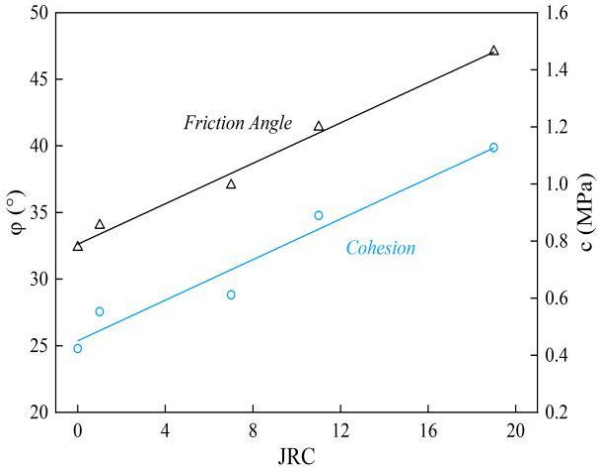

Figure 7 Relationship between JRC and shear strength parameters

3.2 Basic Characteristics of Shear Deformation Curves of Discontinuities with Different JRC.

As illustrated in Figure 8, for the same JRC discontinuity, the higher the normal stress, the higher the peak strength. The stress drop was larger after the peak was over; meanwhile, the overall deformation became smaller, and the shear stiffness increased. When the normal stress was low, the climbing effect was dominant, and the cutting incision effect was weak. The strength component mainly showed the friction strength, and the peak value was not evident for the same JRC. As the normal stress increased, the climbing effect decreased, the incision effect increased, and the peak value became increasingly evident. When the JRC is small, it causes damage and wear out of the discontinuity surface. There was a large stress drop in the curve when the wear accumulated to a certain extent. After the tangential stress reaches the peak point, the discontinuity begins to yield, resulting in a large relative displacement and entering the macroscopic slip stage.

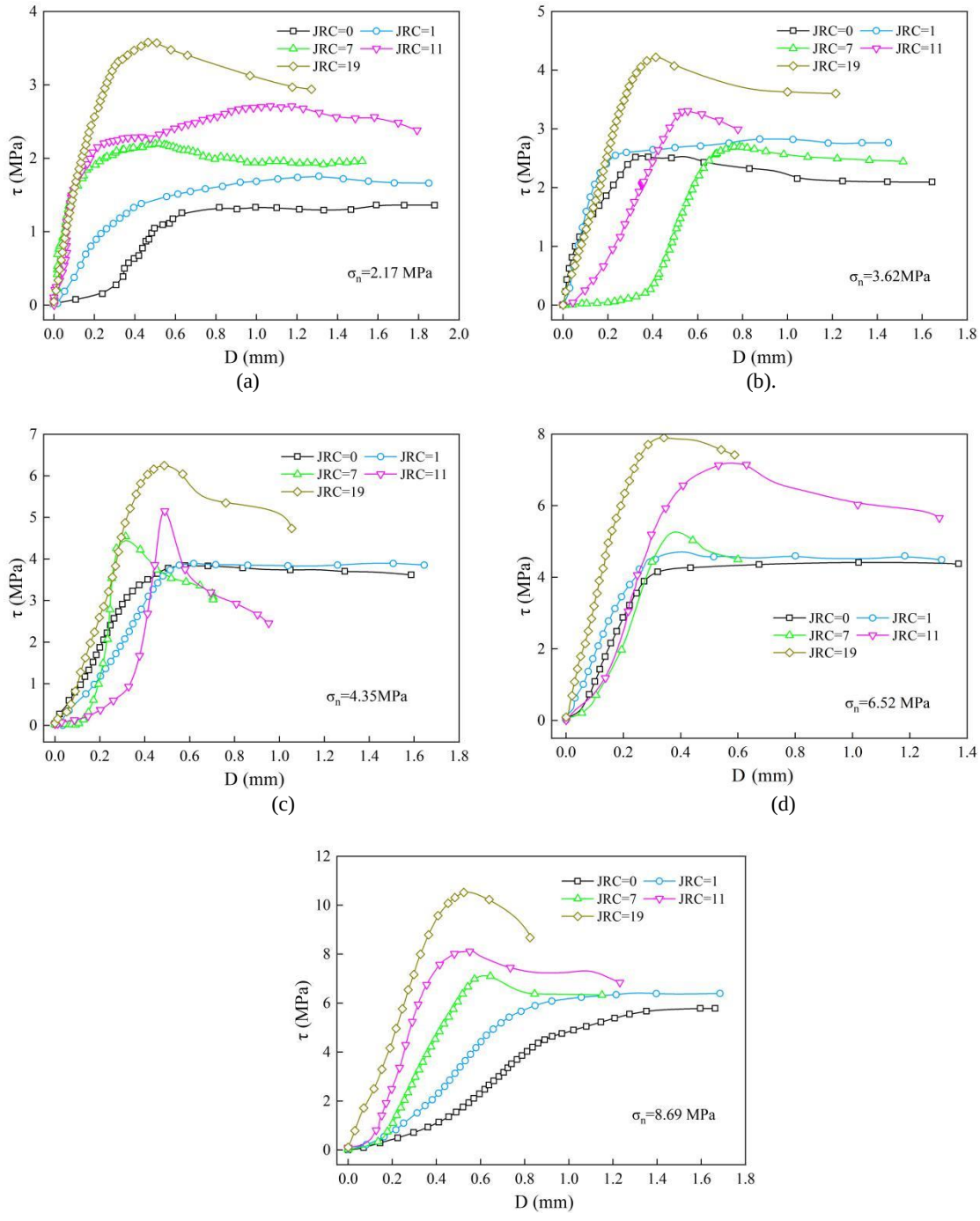

Figure 8. Stress–deformation curve

For the shear deformation curve under the same normal stress (Figure 8), when the JRC is small, the shear curve is generally flatter, because the smaller the roughness of the rock discontinuity, the flatter the rock discontinuity. The shear process is mainly manifested as the friction on the surface of the structural plane, the corresponding shear stiffness is also small, and the shear deformation at the peak stress is larger. When the JRC is large, the "protrusions" of the rock discontinuity are apparent, and the shear process is mainly caused by the protrusions on the surface of the rock discontinuity. As shown in Figure 9(a), when JRC = 19, the protrusions are cut and left in the "grooves" of the rock discontinuity after shear failure. As the shear strength component is mainly manifested as "cutting teeth," the shear

deformation before failure is mainly the deformation of "protruding objects." Compared with the deformation dominated by friction, the allowable relative displacement of rock discontinuity is small, and the shear deformation curve is steeper (i.e., the shear stiffness becomes larger), and the slope of the shear curve changes rapidly after yielding, and the shear stiffness decayed rapidly. However, because the "protrusion" strength is often greater than the friction strength, the shear strength also rapidly increases because of the increase in the "cutting" component. When the JRC is small, as shown in Figure 9(b), the surface morphology after shear failure is mainly abrasion, and no clear shear occurs.

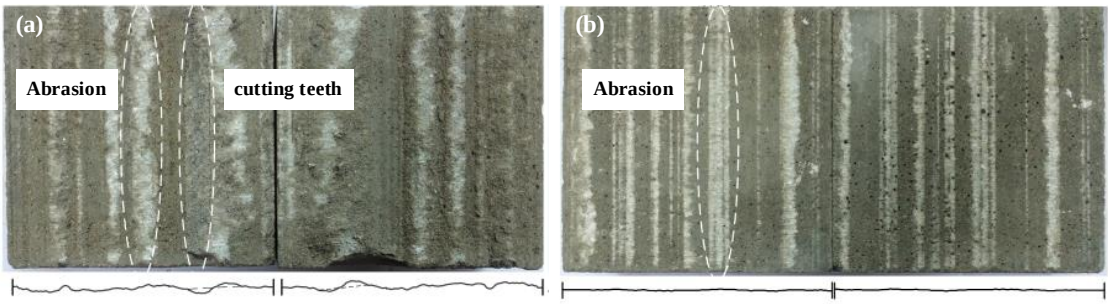

Figure 9. Failure morphology of the sample: (a) JRC=19; (b) JRC=1

3.3 Shear Stiffness Changes During the Shearing

The shear stiffness of the discontinuity was calculated using Equation (1) to study the variation law of the shear stiffness of the discontinuity during shearing.

$$k_S = \frac{\Delta \tau}{\Delta D} \tag{1}$$

The change in the shearing stiffness with deformation is plotted in Figure 10, despite the fluctuations in the shearing stiffness, the basic law is similar. At the initial stage of the shear test, the shear stiffness increases slowly with the increase of shear deformation. This stage corresponds to the compaction stage in the shearing curve (Section OA). Subsequently, the growth rate of shear stiffness increased sharply. This stage corresponds to the first half of the shearing curve (Section AH). When the shearing stress exceeded the stress τ_H corresponding the Point H, the shear stiffness began to decrease. At this time, the stiffness showed a peak (i.e., the sample began to soften after hardening to the limit). As shown in Figure 10, the shear stiffness began to decrease after the stress exceeded τ_H, and it slowly decreased at the beginning and then rapidly decreased, corresponding the Section HB of shearing curve. As shown in Figure 10, Section AB presents an approximately linear form and is the elastic section. When decreased to a certain extent, the shear deformation curve exhibited evident yield characteristics, and the shear stiffness decreased at the highest rate, as shown in the shearing stiffness curve after Point N. This corresponds to Section BC in the shearing curve, which is the yield stage. When the shear deformation reached Point C, the shear stress value was the largest, and the shear stiffness was reduced to zero. When the stress exceeded Point C, the shear deformation curve began to decrease, and the shear stiffness was negative, corresponding to Section CK in Figure 10. The larger the JRC, the better the performance of

this stage. The shear stiffness gradually approaches zero from a negative value as the shear deformation increases.

As afore described, the shear deformation curve of the discontinuity exhibits obvious nonlinear characteristics, and the shear stiffness varies from moment to moment during the shear deformation
progress.

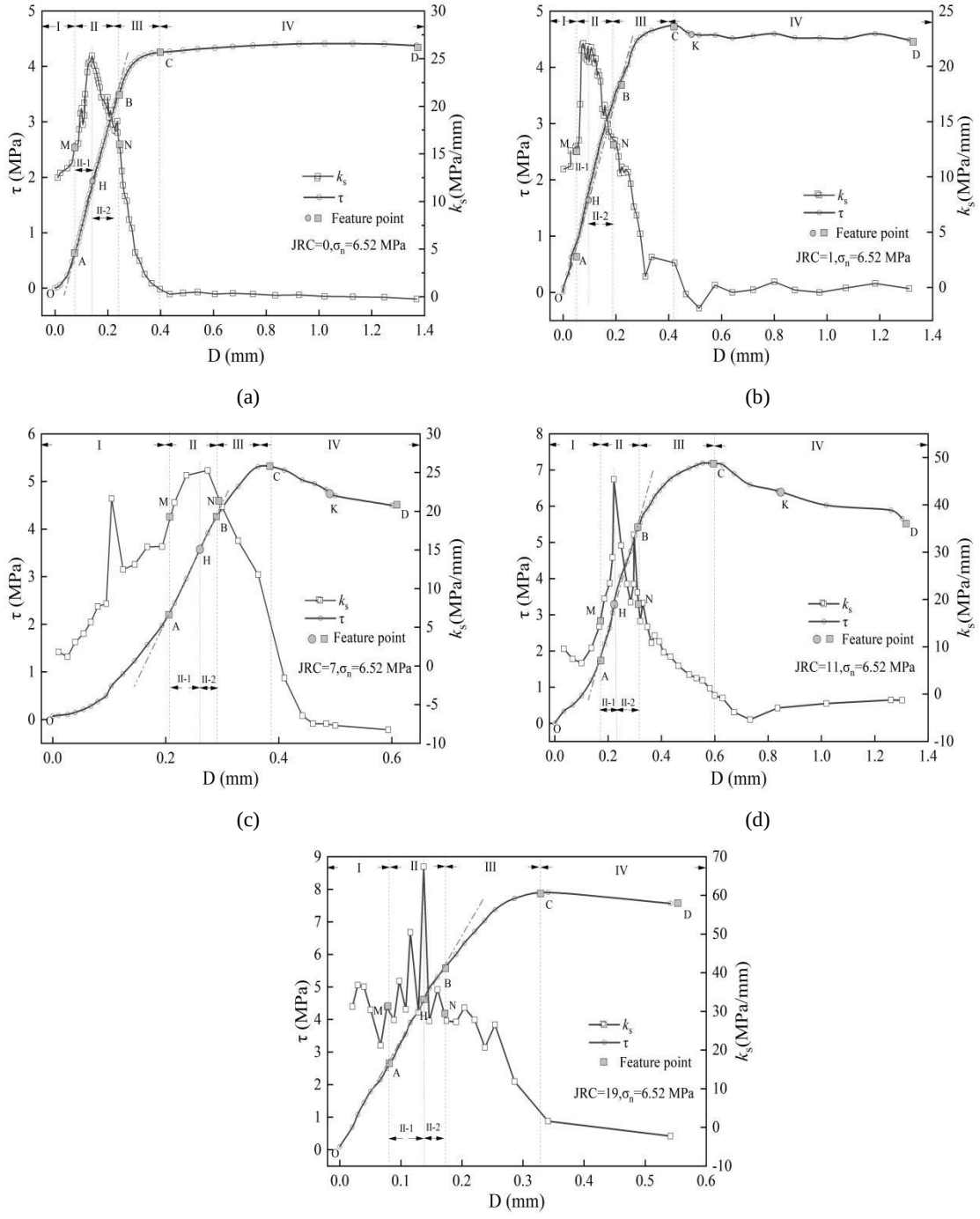

Figure 10. Curve of shear deformation and shear stiffness of rock discontinuity [26]

3.4 Nonlinear Description of Shearing Process of Discontinuity

On the basis of the shearing process of the discontinuities, the rock mass shearing process can be illustrated as shown in Figures 11 and 12. The shearing curve was divided into the following stages based on the variation in the shearing stiffness:

(1) Closure compaction stage (OA): There was a gentle curve before the elastic stage, as shown in Section OA in Figures 10 and 11, which was mainly the contact closure of discontinuities and the gradual closure of microcracks or pores. The specimen was compacted to produce early nonlinear deformation, and the stress-strain curve was concave, with the slope of the curve gradually increasing. At this stage, it was difficult to observe the friction or cutting of teeth on the surface of the discontinuities, whereas a more apparent deformation could be measured.

(2) Stage of elastic deformation and stable development of microcracks (AB): The relationship between the deformation and stress was linear, and the deformation at this stage was also elastic. However, it was not completely linear at this stage from the shear stiffness curve and showed a trend of first increasing and then decreasing, with relatively small changes. It was divided into two stages based on the peak value of the shear stiffness.

(a) Stage of elastic deformation (AH): The shear stress did not reach the cracking stress; therefore, new cracks were not produced, and the contact closure of the discontinuities was completed. For samples with larger JRC, the discontinuities began to cut the protrusion, and the elastic deformation was caused by the horizontal extrusion of the protrusion. Owing to the low stress level, there was elastic deformation in the interior of the discontinuities with no new cracks, causing hardening of the discontinuities, and the shear stiffness increased accordingly. When the JRC was small, the discontinuity mainly overcame the static friction, and the deformation was caused by surface friction and horizontal loading. The stress at Point A was the initial stress at the elastic deformation stage, which was recorded as τ_{cc}.

(b) Stage of micro rupture stable development (HB): When the stress reaches a certain level, new cracks inside the discontinuity begin to appear or the original crack begins to develop. At this stage, new cracks appeared inside the protrusion and started to expand in the shearing direction; however, the crack development was still in a stable stage, and the speed of crack development was not fast. Macroscopically, the shear stiffness of the discontinuity decreases as the rate of decrease gradually increases. The stress at Point H was the stress at which the crack began to occur or expand, and it could be defined as crack stress, which was denoted as τ_{ci}.

(3) Unsteady rupture development stage (BC): The cracks in the protrusion begin to expand, and plastic deformation rapidly increases. The shear deformation curve was no longer an approximately straight line, but an upward convex shape, and this nonlinear morphology rapidly increased with shearing. This is known as the yield stage. The stress concentration effect owing to the development of microfractures caused some of the weakest parts to be destroyed first, followed by stress redistribution. The continuously increasing shear stress damaged the subweak parts, and this process continued until the shear stress reached its peak strength. The stress at Point C was called peak intensity, denoted as τ_s. It was divided into

pre-destruction stage and post-destruction stage by the peak strength point. As shown in Figure 11, the shear stiffness at this stage continues to decrease until it reaches 0. In addition, it can be observed from the entire shear process that the shear stiffness at starting Point B of this stage is essentially the same as that at end Point A of the first stage, and the shear stiffness positions marked by feature points M and N in Figure 11 are the same. This indicates that, under the action of shear stress, when the shear stiffness increases and then decreases to the same shear stiffness as that in the compaction stage, the yield stage begins. The stress at Point B is the yield stress τ_{cd}.

(4) Post-peak strength stage (CD): When the stress is at the peak strength, the fracture gradually penetrates, the protrusion is completely sheared, and the shear strength is reduced to zero. The new discontinuities slid along the new transfixion plane after shearing going on, and the original protrusion was sheared and taken away, in this manner, the protrusion of footwall was cut off and became a part of the upper plate and filled in its depression. This stage is divided into two parts.

(a) Stage of shearing softening (CK): After the peak strength, the stress decreased with an increase in deformation, discontinuities appeared to soften, and the shearing curve exhibited a negative stiffness characteristic. As the control method was stress control, the gear of the test machine rapidly rotated at this stage, and the deformation rapidly increased because of the rapid release of the internal energy of the discontinuities. At this stage, the shearing stiffness rapidly decreases in the negative direction, gradually increases after reaching a certain level, and finally, its distribution becomes horizontal. This stage exists only in the case of a large JRC. No CK stage was observed when JRC = 0. This is because, when JRC = 0, the main deformation mode is friction. The energy was mainly released in the form of friction, and the ability to store energy was weak; therefore, there was no sudden release of energy inside the discontinuities after the peak, and the softening behavior was not distinct.

(b) Stage of flow-slip (KD): With the development of deformation, the discontinuities begin to slide along the new fissure surface, the shearing deformation curve tends to be horizontal, and the shearing stiffness tends to zero. The discontinuities continued slipping under stress, which is called the residual strength, and this stage could be considered as the ideal plastic stage. There was debris between the surfaces of the discontinuities due to friction, reducing the friction effect and decreasing the degree of bite. This was equivalent to the reduction in the JRC (i.e., the discontinuity roughness during the shearing process gradually attenuated with the accumulation of shearing deformation).

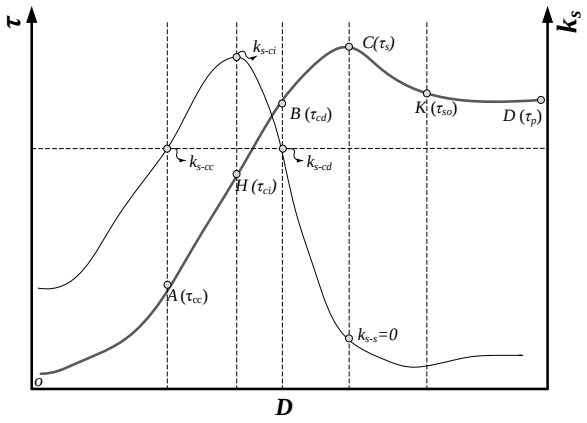

Figure 11. Shear process curve and shear stiffness change characteristics of rock discontinuity

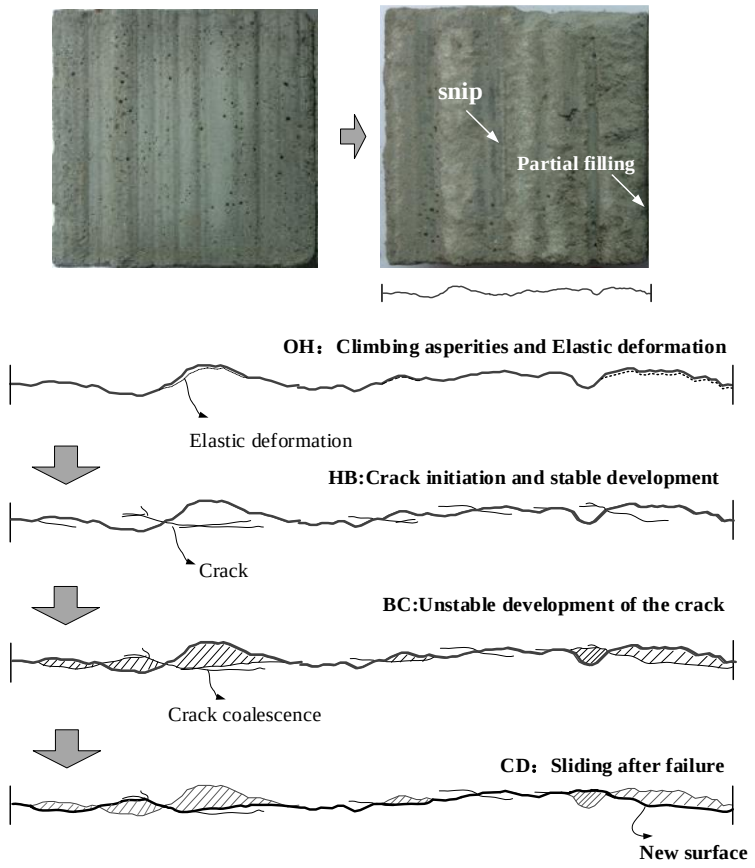

Figure 12. Sketch of shear process of rock discontinuity

3.5 Influence of JRC and Normal Stress on the Nonlinear Shearing Feature Point

The above characteristic points were counted to further study the influence of the JRC and normal stress on the shearing characteristics of the discontinuities, as listed in Table 3. The ratio of yield stress to peak intensity (τ_{cd}/τ_s) indicated the magnitude of stress applied from yielding to failure and the position of yield point in the entire curve. The larger the ratio, the closer the yield points are to the peak strength, and the shorter the process from yield to failure. The value showed a gradual decreasing tendency with a larger JRC and normal stress,

indicating that the stress applied from the yield to damage was large, and the space for the occurrence, development, or plastic deformation of cracks increased after the yield stress.

The ratio of cracking stress to the peak intensity (τ_{ci}/τ_s) indicated the relative position of cracking stress in the whole curve and the length of rising process of shearing stiffness. The higher the shearing stiffness, the longer the energy storage process. As shown in Table 3, when JRC and normal stress was larger, the value of τ_{ci}/τ_s was greater, illustrating that the elastic energy stored in the sample was more.

The ratio of the cracking stress to the yield stress (τ_{ci}/τ_{cd}) showed the speed development of cracks. When the value of τ_{ci}/τ_{cd} was larger, the cracking stress was closer to yield stress. Discontinuities entered the yield stage soon after they cracked inside, which was related to the accumulation of energy before the development of internal cracks. The discontinuities would enter the yield stage faster after cracking when the energy accumulated is higher. The larger the values of JRC and normal stress, the greater the value.

Table 3. Stress values of characteristic points

σ_n (MPa)	JRC	τ_s (MPa)	τ_{cd} (MPa)	τ_{ci} (MPa)	τ_{cd}/τ_s (%)	τ_{ci}/τ_s (%)	τ_{ci}/τ_{cd} (%)
2.17	0	1.36	1.05	0.78	77.21	56.99	73.81
	1	1.76	1.20	0.69	68.18	39.38	57.75
	7	2.20	1.60	1.18	72.73	53.82	74.00
	11	2.71	2.15	1.05	79.34	38.75	48.84
	19	3.58	2.50	2.03	69.83	56.70	81.20
3.62	0	2.55	2.10	1.63	82.35	63.80	77.48
	1	2.83	1.75	1.46	61.84	51.59	83.43
	7	2.70	2.10	1.16	77.78	43.14	55.46
	11	3.31	2.60	1.38	78.55	41.67	53.06
	19	4.22	3.10	2.64	73.46	62.56	85.16
4.35	0	3.84	2.80	2.13	72.92	55.57	76.21
	1	3.89	3.10	2.44	79.69	62.72	78.71
	7	4.54	4.00	3.53	88.11	77.83	88.33
	11	5.15	4.20	3.86	81.55	74.90	91.84
	19	6.25	4.90	4.00	78.40	64.00	81.63
6.52	0	4.41	3.48	1.93	78.80	43.65	55.40
	1	4.73	3.75	1.83	79.28	38.58	48.80
	7	5.31	4.25	3.55	80.04	66.85	83.53
	11	7.19	5.40	3.30	75.10	45.90	61.11
	19	7.90	5.60	4.60	70.89	58.23	82.14
8.69	0	5.80	4.40	3.35	75.86	57.76	76.14
	1	6.42	4.60	3.33	71.65	51.82	72.33
	7	7.16	5.20	3.80	72.63	53.03	73.02
	11	8.11	5.80	4.51	71.52	55.61	77.76
	19	10.54	7.50	6.28	71.16	59.58	83.73

4. Conclusions

In this paper, a series of direct shear tests are carried out on artificial rock discontinuity samples with different roughness under various normal stresses. The influence of roughness on the rock discontinuity strength is studied, the deformation characteristics of the sample during the failure process are analyzed, and the nonlinear characteristics of the rock discontinuity shear process are studied from the perspective of the change of shear stiffness. The mechanism is discussed and the following conclusions are reached:

(1) The rock discontinuity strength increased with increasing roughness and exhibited a good linear relationship.

(2) The higher the roughness, the more apparent the peak value of the shear deformation curve, and the shear mechanism changes with an increase in the JRC, which is manifested by the transition from the wear type to the cutting type.

(3) The shear process of the rock discontinuity underwent four stages: the closing compaction stage of the rock discontinuity and fracture, stable development stage of elastic deformation and microfracture, development stage of unstable fracture, and post-peak segment. These four stages are nonlinear processes. The final effect of shear is that the roughness of the rock discontinuity decreases, and the rock discontinuity tends to flatten.

(4) Before the shear failure, the positions of the shear nonlinear feature points reflect the shape of the shear curve, state of fracture development, and energy storage in the rock discontinuity. With the increase of normal stress and JRC, the energy stored by the sample increases, the rate of fracture development from stable to unstable becomes higher, and the "space" for fracture or plastic deformation to develop increases.

Author Contribution: Pengtao He provided the concept and edited the draft of the manuscript; Chaoran Li developed the idea for the study; Wei Zheng conducted the literature review, tests and wrote the first draft of the manuscript.

Funding: This work was financially supported by the National Natural Science Foundation of China (Grant No. 42002266)

Conflict of interest: The authors declare that they have no conflict of interest.

References:

1 Patton F. Multiple modes of shear failure in rock, in 1st ISRM Congress, September 25–October 1, 1966, Lisbon, Portugal, paper number: ISRM-1CONGRESS-1966-087.

2 Ladanyi B, Archambault G. Simulation of shear behavior of a jointed rock mass, in the 11th U.S. Symposium on Rock Mechanics (USRMS), Berkeley, California, 19 June 1969, paper Number: ARMA-69-0105.

3 Barton N, Choubey V. The shear strength of rock joints in theory and practice. *Rock Mech. Rock Eng.*, 1977, 10(1): 1-54.

4 Barton N, Bandis S. Review of predictive capabilities of JRC-JCS model in the engineering practice. *Rock Joints*, 1990, 603 − 610, DOI: 10.1016/0148-9062(91)90682-c.

5 Goodman R. Introduction to rock mechanics. J. Willey and Sons,1989.

6 Goodman R, Taylor R, Brekke T. A model for the mechanics of jointed rocks. *J. Soil Mech. Found. Div*., 1968, DOI: 10.1061/JSFEAQ.0001133.

7 Ji F, Shi Y. A study of the measuring and strength size effect of the surface shape of structure plane. *Hydrogeol. Eng. Geol.*, 2011, 38(04):63-68. Corpus ID: 112475393

8 Bandis S, Lumsden A, Barton N. Fundamentals of rock joint deformation. *Int. J. Rock mech. Min. Sci. Geomech. Abstr.*, 1983, 20(6): 249-268, DOI: 10.1016/0148-9062(83)90595-8.

9 Barton N, Bandis S, Bakhtar K. Strength, deformation and conductivity coupling of rock joints. *Int. J. Rock mech. Min. Sci. Geomech. Abstr.*, 1985, 22(3): 121-140, DOI: 10.1016/0148-9062(85)93227-9

10 Sharp J , Maini Y , Brekke T .Evaluation Of Hydraulic Properties Of Rock Masses[J].helsingin yliopisto, 1972. DOI:10.1068/p020441.

11 Sun Z. Fracture mechanics and tribology of rocks and rock joints. Doctoral thesis, Lulea: Lulea University of Technology, Sweden, 1983.

12 Malama B, Kulatilake P. Models for normal fracture deformation under compressive loading. *Int. J. Rock Mech. Min. Sci.*, 2003, 40(6): 893-901, DOI: 10.1016/S1365-1609(03)00071-6

13 Zhao J, Cai J, Zhao X, Song H. Transmission of elastic p-waves across since fracture with nonlinear normal deformation behavior. *Chin. J. Rock Mech. Eng.*, 2003, 22(1):9-17, DOI: 10.1007/s006030170023.

14 Jing L, Nordlund E, Stephansson O. A 3-D constitutive model for rock joints with anisotropic friction and stress dependency in shear stiffness. *Int. J. Rock mech. Min. Sci. Geomech. Abstr*., 1994, 31(2): 173-178, DOI: 10.1016/0148-9062(94)92808-8

15 Yin X, Wang J, Zhang C. Study of constitutive model for rock interfaces and joints under cyclic shear loading. Eng. Mech., 2005, 22(6): 97-103. (In Chinese)

16 Du S, Zhu J, Zhi H. Shear tests on rock joints under different shear deformation histories. *Chin. J. Rock Mech. Eng.*, 2006, 25(1):56-60. (In Chinese)

17 Huang D, Huang R, Lei P. Shear deformation and strength of through-going saw-ooth rock discontinuity. *J. China Coal Soc*., 2014, 07: 1229-1237. (In Chinese)

18 Barton N, Bakhtar K, Bandis S .Rock Joint Description and Modelling for Prediction of Near-Field Repository Performance[J]. Mrs Proceedings, 1983, 26:1047. DOI:10.1557/PROC-26-1047.

19 Barton N. Suggested methods for the quantitative description of discontinuities in rock masses. ISRM, *Int. J. Rock mech. Min. Sci. Geomech. Abstr.*, 1978, 15(6). 319-368.

20 Du S, Huang M, Luo Z, et al. Similar material study of mechanical prototype test of rock structural plane. *Chin. J. Rock Mech. Eng.*, 2010, 29(11): 2263-2270. (In Chinese)

21 Einstein H, Veneziano D, Baecher G, et al. The effect of discontinuity persistence on rock slope stability. *Int. J. Rock mech. Min. Sci. Geomech. Abstr*.1983, 20(5): 227-236.

22 Li H, Feng H, Liu B. Study on strength behaviors of rock joints under different shearing deformation velocities. *Chin. J. Rock Mech. Eng.*, 2006(12): 2435-2440. (In Chinese)

23 Shen M, Zhang Q. Experimental study of shear deformation characteristics of rock mass discontinuities. *Chin. J. Rock Mech. Eng.*, 2010, 29(04): 713-719. (In Chinese)

24 Wang Z, Shen M, Ding W, et al. Time-dependent behavior of rough discontinuities under shearing conditions. *J. Geophys. Eng.*, 2018, 15(1): 51, DOI: 10.1088/1742-2140/aa83e9.

25 Bandis S, Lumsden A, Barton N. Experimental studies of scale effects on the shear behaviour of rock joints. *Int. J. Rock mech. Min. Sci. Geomech. Abstr*. 1981, 18(1): 1-21.

26 Gu L, Wang Z, Zhang F, et al. Dynamic evolution of shear rate-dependent behavior of rock discontinuity under shearing condition. *J. Cent. South Univ.*, 2021, 28(6): 1875-1887, DOI: 10.1007/s11771-021-4736-4